Principal Geodesic Analysis applied to climate time series

Nozomi Sugiura

Research Institute for Global Change, JAMSTEC, Japan

04 April 2023

Abstract

Principal Geodesic Analysis (PGA) is applied to a climate time series. First, we transform each multidimensional sequence into the path signature. Since the signature lives in a curved space, usual principal component analysis (PCA) is not applicable. Instead, we treat the signature space as a geodesic manifold. By replacing the notion of straight lines with that of geodesics, the domain of PCA can be extended to the curved space. Then, the first principal component is derived as the geodesic that minimizes the unexplained variance in the data. As an application, we computed the leading modes for one-year NINO SST time series, which are divided into segments that represent annual variations of monthly averages. It is interesting that some months in a year reveal characteristic undulations that could indicate the early signs of upcoming El Ninõ events.

1 Introduction

The usefulness of the principal component analysis (PCA; Pearson (1901)) in data analysis is indisputable. In particular, it has been used in the earth sciences to extract characteristic structures within observational data sets. In this field, it is also called the EOF analysis (e.g., Stephenson and Benestad, 2000).

On the other hand, multidimensional sequential data, such as time series data and profile observation data, frequently appear in data analysis. It is known that such sequential data can be efficiently represented as paths by converting them into tensors called signatures (e.g., Lyons et al., 2007). Signature spaces are known to have rich algebraic and geometric structures, especially as a Lie group (e.g., Friz and Victoir, 2010).

Principal component analysis on the data constituting Lie groups has been vigorously investigated by Pennec and his group (e.g., Pennec and Lorenzi, 2020). It is essential that geodesics be made concrete rather than introducing specific connections to Lie groups. This makes the principal geodesic analysis (PGA) by Fletcher et al. (2004) feasible for structured data.

Although there have been several attempts to analyze geophysical data in a nonlinear framework, which include Gámez et al. (2004), no consistent approach on a rigorous basis can be found so far.

In this study, we describe how to apply PGA to sequential data through signature transformation. We also illustrate its usefulness by applying PGA to real climate time series (NOAA, 2021).

2 Theoretical background

2.1 Signatures constitute a Lie group

- A path is a function with bounded variation from unit interval $[0,1] \subset \mathbb{R}$ to $\mathbb{R}^d$, defined as $X : t \mapsto (X_t^{(1)}, \cdots, X_t^{(d)})$. The 0-th and 1-st iterated integrals (e.g., Lyons et al., 2007; Friz and Victoir, 2010) of path X are defined as

$$\mathcal{S}^{()}(X)_{0,t} = 1, \tag{1}$$

$$\mathcal{S}^{(i)}(X)_{0,t} = \int_0^t dX_s^{(i)} = X_t^{(i)} - X_0^{(i)}, \quad i = 1, \cdots, d. \tag{2}$$

For $k = 2, 3, \cdots$, the k-th iterated integral is defined recursively as

$$\mathcal{S}^{(i_1 \cdots i_k)}(X)_{0,t} = \int_0^t S^{(i_1 \cdots i_{k-1})}(X)_{0,s} dX_s^{(i_k)}, \tag{3}$$

where $i_1, \cdots, i_k = 1, \cdots, d$.

- Then, step-n signature x (e.g., Lyons et al., 2007; Friz and Victoir, 2010) is defined as an element of tensor algebra:

$$\mathcal{T}_n(\mathbb{R}^d) = \bigoplus_{k=0}^{n} (\mathbb{R}^d)^{\otimes k} \ni x = 1 + \sum_{i_1=1,\cdots,d} x^{(i_1)} e_{i_1} + \cdots + \sum_{i_1,\cdots,i_n=1,\cdots,d} x^{(i_1\cdots i_n)} e_{i_1} \cdots e_{i_n}, \quad (4)$$

where $x^{(i_1\cdots i_k)} = \mathcal{S}^{(i_1\cdots i_k)}(X)_{0,1}$ is the iterated integral of path X, and e_i is the basis of $\mathbb{R}^d$.

1. The I-th coordinate for the signature is $x^{(I)}$, where I is a multi-index. In this sense, we can regard $x \in \mathbb{R}^N$, $N = 1 + d + \cdots + d^n = (d^{n+1} - 1)/(d - 1)$.
2. Since the iterated integrals should satisfy the shuffle relation (e.g., Lyons et al., 2007) , e.g. $x^{(1)}x^{(2)} = x^{(12)} + x^{(21)}$, the signatures are located in a limited area in $\mathbb{R}^N$.

This implies that the set of order-n signature has a manifold structure (not flat).

- Signature is also an element of a group G. Indeed, if we define the group operation for elements

$$x = \mathcal{S}_n(X) = 1 + \sum_{k=1}^{n} \sum_{i_1,\cdots,i_k=1,\cdots,d} x^{(i_1\cdots i_k)} e_{i_1} \cdots e_{i_k}$$

and

$$y = \mathcal{S}_n(Y) = 1 + \sum_{k=1}^{n} \sum_{i_1,\cdots,i_k=1,\cdots,d} y^{(i_1\cdots i_k)} e_{i_1} \cdots e_{i_k}$$

as

$$xy = 1 + \sum_{k=1}^{n} \sum_{i_1,\cdots,i_k=1,\cdots,d} \left(\sum_{j=0}^{k} x^{(i_1\cdots i_j)} y^{(i_{j+1}\cdots i_k)} \right) e_{i_1} \cdots e_{i_k},$$

then G has

1. Product: If $x, y \in G$, then $xy = \mathcal{S}_n(X * Y) \in G$, where $*$ is the concatenation of paths.
2. Unit: $e = \mathcal{S}_n(\bullet) = 1 \in G$ that satisfies $ex = xe = x$, where $\bullet$ is a point.
3. Inverse: $x^{-1} = \mathcal{S}_n(\overleftarrow{X}) \in G$ that satisfies $x^{-1}x = xx^{-1} = e$, where $\overleftarrow{X}$ is the path in the opposite direction.

- Since the signatures are in both Group and Manifold, they form a Lie group.

- For $x \in G$, we define logarithm map $\log(x) := \sum_{k=1}^{n} (-1)^{k-1} \frac{(x-1)^k}{k} \in \log G$ with respect to the group operation. Then, we find that $u, v \in \log G$ is closed under linear combination $\alpha u + \beta v \in \log G$, $\alpha, \beta \in \mathbb{R}$, and commutator product $[u, v] = uv - vu \in \log G$ (e.g., Chapter 7 of Friz and Victoir, 2010). With such Lie algebra structure, $\log G$ is identified with the tangent space at the origin T_eG, which is also called the log-signature space $\mathfrak{g}$. Conversely, for $v \in T_eG$, we can define the exponential map by $\exp(v) := \sum_{k=1}^{n} \frac{v^k}{k!} \in G$ with respect to the group operation.

- A simple example with $n = 2$, $d = 2$ is as follows.
  - **Signature space** G is a 3-dimensional manifold embedded in $\mathbb{R}^6$:

$$G = \left\{ 1 + x^{(1)}e_1 + x^{(2)}e_2 + x^{(11)}e_{11} + x^{(12)}e_{12} + x^{(21)}e_{21} + x^{(22)}e_{22} \middle| x^{(i)}x^{(j)} = x^{(ij)} + x^{(ji)} \right\}$$
$$\cong \left\{ \left(a, b, \frac{a^2}{2}, \frac{ab}{2} + c, \frac{ab}{2} - c, \frac{b^2}{2} \right) \middle| a, b, c \in \mathbb{R} \right\}.$$

    Moreover, it is easy to see that if $x, y \in G$, then $xy \in G$ and $x^{-1} \in G$.
  - **Log-signature space** $\mathfrak{g}$ is a 3-dimensional vector space:

$$\mathfrak{g} = \left\{ x^{(1)}e_1 + x^{(2)}e_2 + \frac{x^{(12)} - x^{(21)}}{2}(e_{12} - e_{21}) \right\} \cong \{(a, b, c) | a, b, c \in \mathbb{R}\}.$$

    Moreover, it is easy to see that if $u, v \in \mathfrak{g}$, then $[u, v] \in \mathfrak{g}$.
  - Therefore, G is regarded as a 3-dimensional manifold (not necessarily endowed with a Riemannian metric), and furthermore a Lie group.

2.2 Motivation toward Pennec's theory

- It is not possible to define a bi-invariant metric for most Lie groups (Pennec and Arsigny, 2013), including the signature space.
- On the other hand, since the tangent PCA (Fletcher et al., 2004) uses data point itself as an approximation to its projection onto the principal mode, a more accurate method is needed in some cases.
- It is notable that without using a metric we can extend the notion of principal component analysis to a curved space. In that geometry, the only thing we should employ is geodesics.
- By replacing straight lines to geodesics, we can perform the principal geodesic analysis (PGA) (Fletcher et al., 2004; Sommer et al., 2014) instead of PCA.

2.3 Essence of Pennec's theory

- A geodesic $\gamma(t)$ satisfies $\nabla_{\dot\gamma(t)}\dot\gamma(t) = 0$ (auto-parallel). In particular, we consider geodesics starting from origin $\gamma(0) = e$.
- A 1-parameter subgroup $\beta(t)$ starting from origin e is determined by $\dot\beta(0) = X \in T_eG$, and written as $\beta(t) = \exp(tX)$, using the exponential map of the Lie group G. It is an integral curve of the left-invariant vector field $\tilde X$ determined by $X \in T_eG$.
- We assume that the manifold is endowed with a Cartan-Schouten connection (CSC): $\nabla_{\tilde X}\tilde Y = \frac{1}{2}[\tilde X, \tilde Y]$, which satisfies $\nabla_{\tilde X}\tilde X = 0$.
- This connection is bi-invariant; namely, the translation of $\tilde X$ and $\tilde Y$ is equivalent to that of $\nabla_{\tilde X}\tilde Y$:

$$\nabla_{dL_m\tilde X} dL_m\tilde Y = dL_m(\nabla_{\tilde X}\tilde Y), \quad \nabla_{dR_m\tilde X} dR_m\tilde Y = dR_m(\nabla_{\tilde X}\tilde Y).$$

- Under the CSC, the geodesic from the origin with initial velocity $\dot\gamma(0) = X$ coincides with the 1-parameter subgroup $\beta(t)$.
- Therefore, we can write the geodesic as $\gamma(t) = \beta(t) = \exp(tX)$.
- Also, a geodesic starting from $m \in G$ with initial velocity $U \in T_mG$ is written as $\gamma(t) = L_m \exp(tdL_{m^{-1}}U)$.

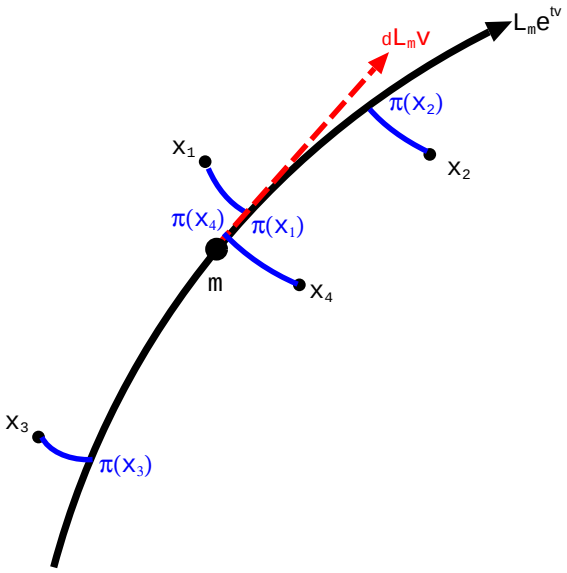

Figure 1: Concept of Principal Geodesic Analysis. Black and blue curves are geodesics. Vector v is chosen to minimize the unexplained variance $\sum_\ell d^2(\pi(x_\ell), x_\ell)$, where $\pi(x_\ell) = me^{t_\ell v}$.

2.4 Group mean

- Suppose we have data points $\{x_\ell | \ell = 1, \cdots, L\}$.
- Group mean m satisfies $\nabla_m \sum_{\ell=1}^L d^2(m, x_\ell) = (-2)m \sum_{\ell=1}^L \log(m^{-1}x_\ell) = 0$.

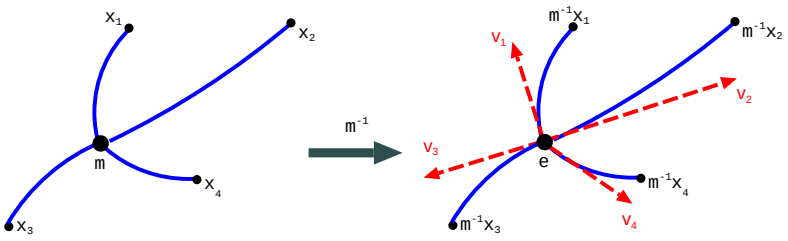

Figure 2: In the right fig., the blue curves are geodesics $\gamma(t) = \exp(t \log(m^{-1}x_\ell))$. Group mean m is chosen so that the tangent vectors $v_\ell = \log(m^{-1}x_\ell)$ at the origin are in balance. Locally, it is equivalent to minimizing $\sum_\ell d^2(m, x_\ell)$.

Fréchet (1948) defined the mean m of data $\{x_\ell\}_{\ell=1}^L$ as

$$m = \arg\min_{m \in G} \sum_{\ell=1}^{L} d^2(m, x_\ell). \tag{5}$$

Notice that the gradient of the squared distance has an explicit form:

$$\nabla_m d^2(m, x) = -2 \operatorname{Log}_m x, \tag{6}$$

where $\mathrm{Log}_m x$ represents the initial velocity $\dot{\gamma}(0)$ of the geodesic from $\gamma(0) = m$ to $\gamma(1) = x$. See Appendix A for derivation. Using this, Karcher (1977) characterized the mean as a stationary point:

$$\nabla_m \sum_{\ell=1}^{L} d^2(m, x_\ell) = \sum_{\ell=1}^{L} (-2) \,\mathrm{Log}_m x_\ell = 0, \tag{7}$$

In the case where x and m are in the signature space G equipped with the CSC, we have $\mathrm{Log}_m x = m \log(m^{-1}x)$. Therefore, Eq. (7) reads

$$\sum_{\ell=1}^{L} \log(m^{-1}x_\ell) = 0. \tag{8}$$

Equation (8) characterizes the group mean m, and it can be solved by fixed-point iteration:

$$m^{\mathrm{new}} = m \exp\left(\frac{1}{L}\sum_{\ell=1}^{L} \log(m^{-1}x_\ell)\right). \tag{9}$$

2.5 Tangent PCA

A method termed tangent PCA goes as follows.

- In the procedure for deriving the group mean (Fig. 2), the tangent vectors, $\{v_\ell := \log(m^{-1}x_\ell)\}_{\ell=1,\cdots,L}$, are considered as the linearized set of data.
- The eigenvalue decomposition of "covariance matrix", $C = \frac{1}{L}\sum_{\ell=1}^{L} v_\ell \otimes v_\ell$, is performed to have several principal modes of the data.

2.6 Principal Geodesic Analysis

More rigorous method than tangent PCA is termed Principal Geodesic Analysis (PGA), which goes as follows.

- Suppose we have data $\{x_\ell\}_{\ell=1,\cdots,L}$ with their group mean m.
- We draw a geodesic, equivalently 1-parameter subgroup, passing through m. In the case of signature, it reads

$$\gamma_v(t) = m \exp(tv). \tag{10}$$

- We project each data x_ℓ onto the geodesic. The projected point is written as $\pi_v(x_\ell) = \gamma_v(t_\ell)$ with an appropriate t_ℓ.
- Then, we find the vector $v \in T_eG$ of the geodesic that minimizes the distance from the data point to the projected point (Guigui et al., 2023).

$$v = \arg\min_v \sum_{\ell=1}^{L} d^2(\pi_v(x_\ell), x_\ell). \tag{11}$$

- Since the summation in (11) is the variance that the geodesic cannot explain, we call it the unexplained variance.
- In this regard, the geodesic determined by (11) can be regarded as the mode that best describe the data.

2.7 Stationary value problem

We have data $\{x_\ell\}_{\ell=1,\cdots,L}$ with their group mean m. We want to find the modes that minimize the unexplained variance in a geodesic space.

1. We project data x_ℓ onto the geodesic passing through the mean m; the projected point is $\pi(x_\ell) = m\exp(t_\ell v)$. Then, find the initial velocity v of the geodesic that minimizes the distance from the data point to the projected point.

$$\forall \ell) \quad t_\ell = \underset{t_\ell \in \mathbb{R}}{\arg\min}\, d^2(m\exp(t_\ell v), x_\ell), \tag{12}$$

$$v = \underset{v}{\arg\min} \sum_{\ell=1}^{L} d^2(m\exp(t_\ell v), x_\ell). \tag{13}$$

   Note that the solution to this problem is invariant under the dilation to the signature (See Appendix C).

2. When the signature space is regarded as a geodesic manifold, we don't have explicitly the distance, but its gradient, $\nabla_y d^2(y,x) = -2\,\mathrm{Log}_y x$. Therefore, without using a distance, we can solve it as a stationary value problem:

$$\forall \ell) \quad \nabla_{t_\ell} d^2(m\exp(t_\ell v), x_\ell) = 0, \tag{14}$$

$$\nabla_v \sum_{\ell=1}^{L} d^2(m\exp(t_\ell v), x_\ell) = 0. \tag{15}$$

2.8 PCA as a special case of PGA

We want to minimize the unexplained variance in Euclidean space.

- The squared distance is $d^2(m, x_\ell) = |m - x_\ell|^2$. The gradient of squared distance is $\nabla_m d^2(m, x_\ell) = (-2)(x_\ell - m)$.
- Therefore, the mean should satisfy $\nabla_m \sum_{\ell=1}^{L} d^2(m, x_\ell) = (-2)\sum_{\ell=1}^{L}(x_\ell - m) = 0$, which is solved by $m = L^{-1}\sum_{\ell=1}^{L} x_\ell$.
- According to Eqs. (18) and (19), the first mode v and coefficients $\{t_\ell\}$ are derived through iterations:

$$\forall \ell) \quad t_\ell^{\mathrm{new}} = \frac{\langle v, x_\ell - m\rangle}{|v|^2}, \tag{16}$$

$$v^{\mathrm{new}} = \frac{\sum_{\ell=1}^{L} t_\ell (x_\ell - m)}{\sum_{\ell=1}^{L} t_\ell^2}. \tag{17}$$

- Solution v coincides with the first eigenvector of covariance matrix [1]: $C = L^{-1}\sum_{\ell=1}^{L}(x_\ell - m)(x_\ell - m)^\top$.

[1] It is not the case in curved spaces.

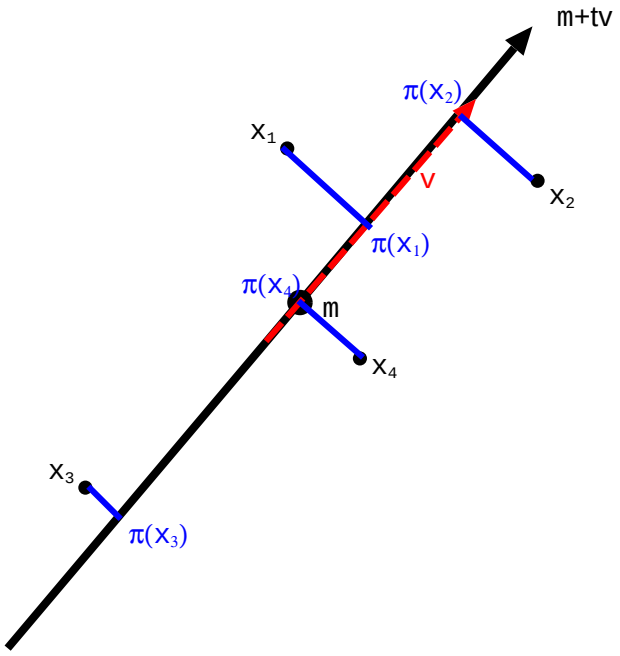

Figure 3: Concept of Principal Component Analysis. Black and blue curves are straight lines. Vector v is chosen to minimize the unexplained variance $\sum_\ell d^2(\pi(x_\ell), x_\ell)$, where $\pi(x_\ell) = m + t_\ell v$.

3 Methods

3.1 Climate Data

The theory will be demonstrated by using climate data from NOAA (NOAA, 2021). The spatio-temporal data to be processed are the following.

- We use time series $\{x_\ell\}_{\ell=1}^L$, each of which is 4-dimensional path, consisting of 13 points of monthly mean value (January to the next January).
- Number of time series is 121 for year 1900 to 2020.
- We use the monthly mean values of sea surface temperature over the El Ninô monitoring regions (See Fig. 15), which are defined as 0° to 10°South and 90°West to 80°West, 5°North to 5°South and 150°West to 90°West, 5°North to 5°South and 160°East to 150°West for NINO1+2, 3, and 4,respectively.
- We define $x_\ell^{(0)} =$ time, $x_\ell^{(1)} =$ NINO1+2, $x_\ell^{(2)} =$ NINO3, and $x_\ell^{(3)} =$ NINO4 for each sample ℓ.
- Each time series is converted into step-4 signature. Thus, the dimension for signature is $N = (4^{4+1} - 1)/(4 - 1) = 341$.

3.2 Problem setting

1. The first mode
   The first mode v is derived by solving the following stationary value problems.

$$\forall \ell) \quad \nabla_{t_\ell} d^2(m \exp(t_\ell v), x_\ell) = 0, \tag{18}$$

$$\nabla_v \sum_{\ell=1}^{L} d^2(m \exp(t_\ell v), x_\ell) = 0. \tag{19}$$

2. The second mode
   Similarly, the second mode v' is derived by solving the following stationary value problems.

$$\forall \ell) \quad \nabla_{t'_\ell} d^2(m \exp(t_\ell v + t'_\ell v'), x_\ell) = 0, \tag{20}$$

$$\nabla_{v'} \sum_{\ell=1}^{L} d^2(m \exp(t_\ell v + t'_\ell v'), x_\ell) = 0, \tag{21}$$

   where we assume v and $\{t_\ell\}$ are already derived by solving Eqs. (18) and (19). This amounts to finding the best projections onto the best 2-dimensional span $\{v, v'\}$ in T_eG.

3.3 Gradient Descent

1. To solve the optimization problem, we need the derivatives of squared distance with respect to t and v. This is done by using automatic differentiation in embedding space $\mathbb{R}^N$, $N = (d^{n+1}-1)/(d-1)$, as described in Appendix D.

2. The first mode is solved by the following iterations. Initially, v is set to the first tangent PC.

$$\forall \ell) \quad t_\ell^{\text{new}} = t_\ell - \epsilon v^\top (\partial \exp|_{t_\ell v})^\top P (\partial_2 \text{prod}|_{m,\exp(t_\ell v)})^\top (-2) p_\ell \log\left(p_\ell^{-1} x_\ell\right), \tag{22}$$

$$v^{\text{new}} = v - \epsilon' P \sum_{\ell=1}^{L} t_\ell (\partial \exp|_{t_\ell v})^\top P (\partial_2 \text{prod}|_{m,\exp(t_\ell v)})^\top (-2) p_\ell \log\left(p_\ell^{-1} x_\ell\right), \tag{23}$$

   where $P := C^\dagger C$, $p_\ell := m \exp(t_\ell v)$. The reasoning for this setting is detailed below.

3. The transposed derivatives of two maps $u \mapsto \exp(u)$ and $u, w \mapsto u \cdot w$, where $\cdot$ is the product in the tensor algebra, can be derived by using the automatic differentiation (adjoint operator) of $(\partial_u \exp|_u)^\top$ and $(\partial_2 \text{prod}|_{u,w})^\top$ in $\mathbb{R}^N$.

4. For the derivetives to stay on the manifold, we set

$$\nabla_v d^2(m e^{tv}, x) = C^\dagger C (\partial_v d^2(m e^{tv}, x))^\top \in T_eG, \tag{24}$$

$$C = \frac{1}{L} \sum_{\ell=1}^{L} u_\ell u_\ell^\top, \tag{25}$$

$$u_\ell = \log\left(m^{-1} x_\ell\right) \in T_eG, \tag{26}$$

   where C is the covariance matrix for the data, and $C^\dagger$ is its pseudo-inverse. $C^\dagger C$ projects the derivative onto span $\{u_1, \cdots, u_L\}$. Since u_ℓ's are legitimate log-signatures that belong to the Lie algebra, so the update is.

5. Furthermore, our climate data have enough dimension: $\text{rank}(C) = 89$, which is comparable to that for the algebra of log-signatures: $\dim(\mathfrak{g}_4(\mathbb{R}^4)) = 90$ (cf. Reizenstein, 2017, Table 2). The degeneracy by one is due to the constant first iterated integral corresponding to the time interval common to the samples.

6. After all, the solution of Eq. (19) is found by minimizing scalar

$$[\partial_v d^2(m e^{tv}, x)] C^\dagger C [\partial_v d^2(m e^{tv}, x)]^\top.$$

7. Similar solution procedure is employed for the 2nd mode.

4 Results

4.1 Principal modes

We draw typical time series that correspond to the eigen modes of the signatures. Before the analysis, each path $X_\ell : [0,1] \to \mathbb{R}^4$ is converted into the step-4 signature $x_\ell = \mathcal{S}_4(X_\ell) \in \mathcal{T}_4(\mathbb{R}^4)$. In the following, v_j is the vector for the j-th mode, and σ_j is the standard deviation of intensities in the j-th mode.

- **PCA** in $\mathbb{R}^{341}$ (control case)

- Mean (black): $m = L^{-1} \sum_{\ell=1}^{L} x_\ell$.
- First modes (red): $m \pm \sigma_1 v_1$.
- First and second modes (blue or purple): $m \pm \sigma_1 v_1 \pm \sigma_2 v_2$.

- **PGA** in Lie group
  - Group mean (black): m, such that $\sum_{\ell=1}^{L} \log(m^{-1} x_\ell) = 0$.
  - First modes (red): $m \exp(\pm \sigma_1 v_1)$.
  - First and second modes (blue or purple): $m \exp(\pm \sigma_1 v_1 \pm \sigma_2 v_2)$.

After the analysis, each signature is converted back into a path. The first two principal modes in PCA are shown as multi-dimensional time series in Figs. 4,5,6,7, and 8. On the other hand, The first two principal geodesic modes are shown as mufti-dimensional time series in Figs. 9,10,11,12, and 13.

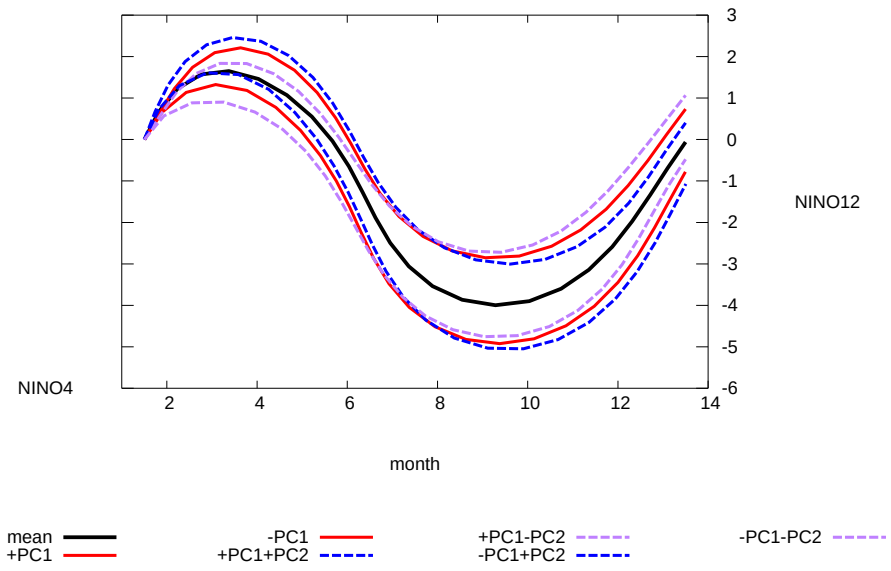

Figure 4: Principal modes in PCA viewed as NINO1+2 time series

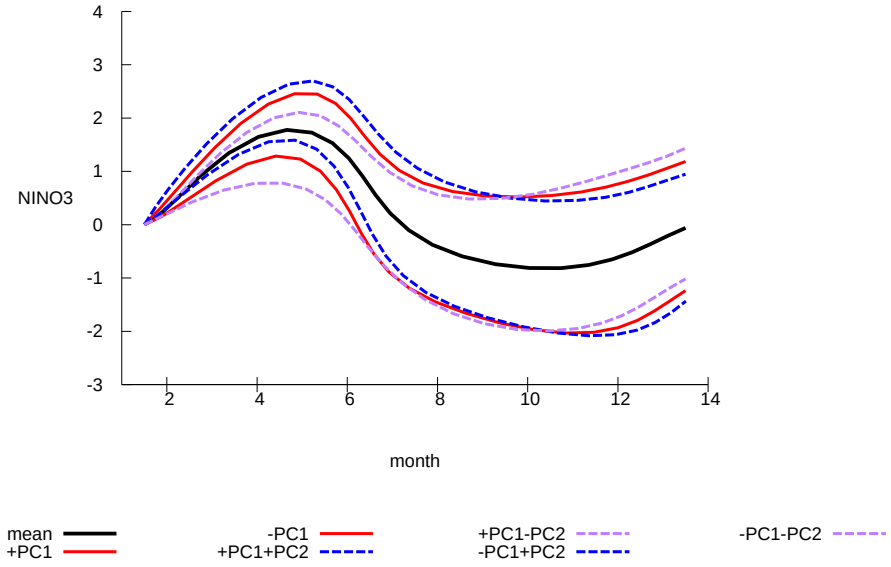

Figure 5: Principal modes in PCA viewed as NINO3 time series

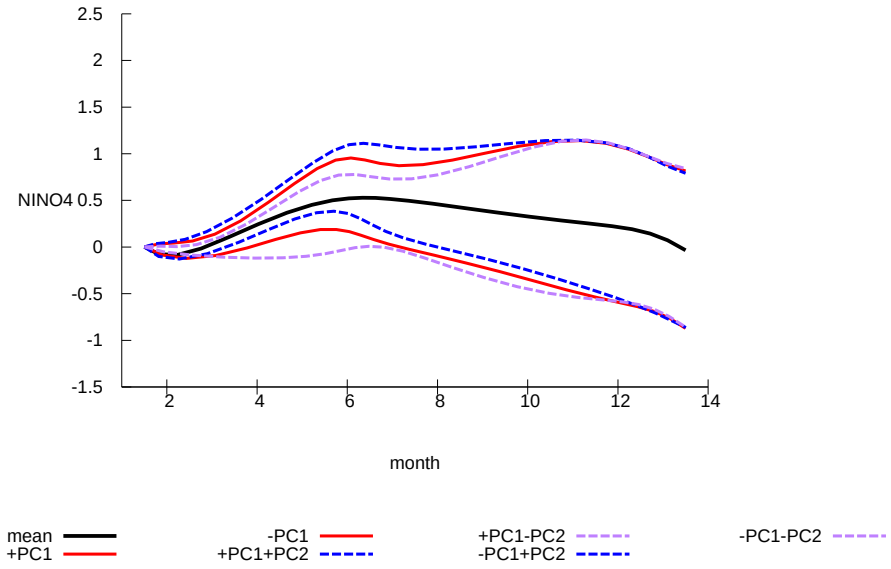

Figure 6: Principal modes in PCA viewed as NINO4 time series

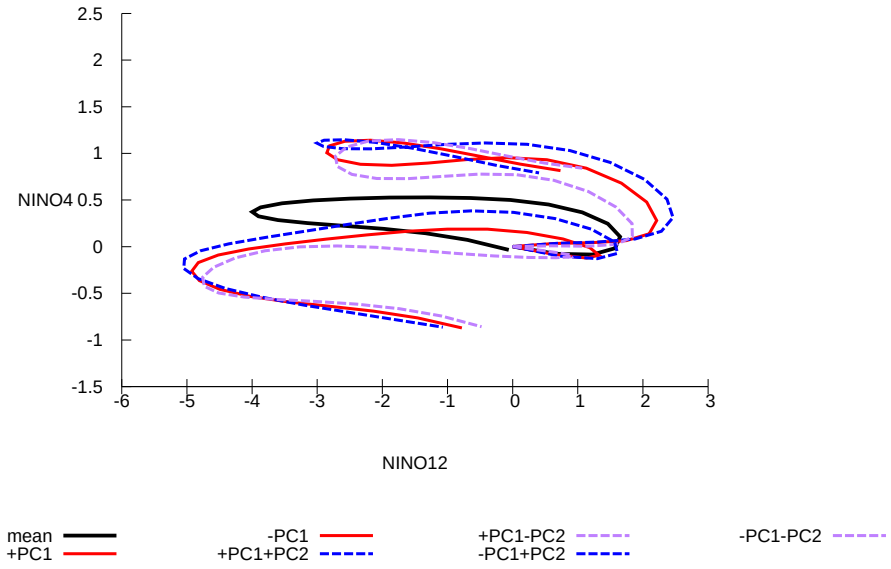

Figure 7: Principal modes in PCA viewed as NINO12vs4 time series

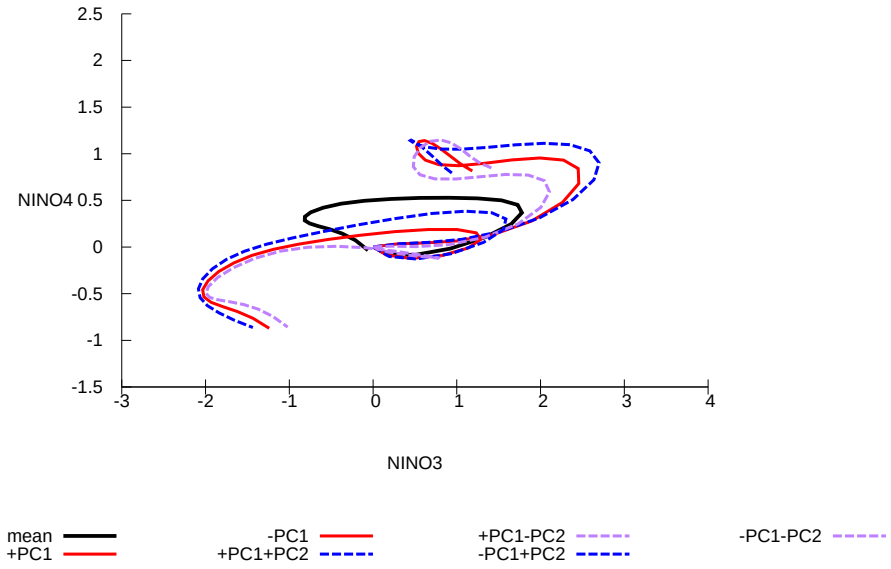

Figure 8: Principal modes in PCA viewed as NINO3vs4 time series

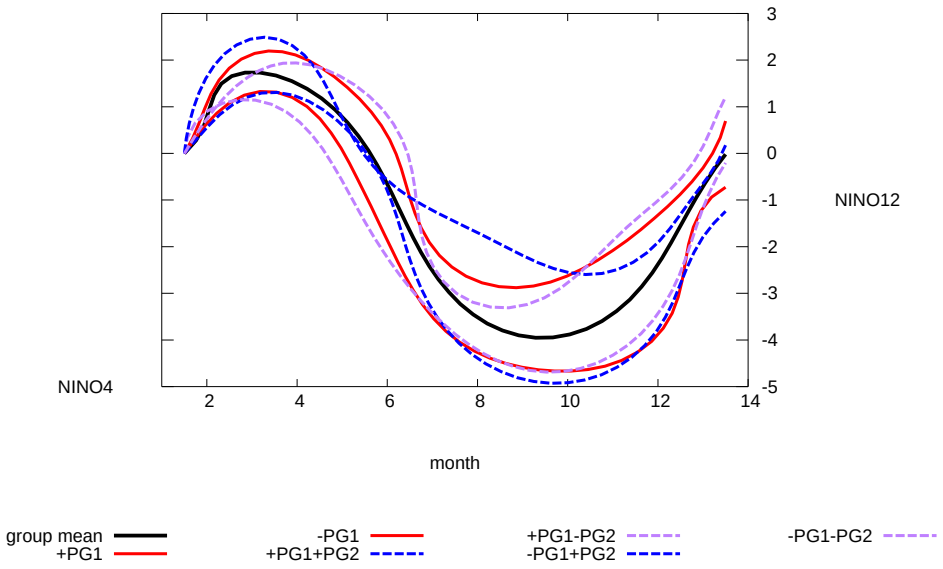

Figure 9: Principal Geodesic modes viewed as NINO1+2 time series

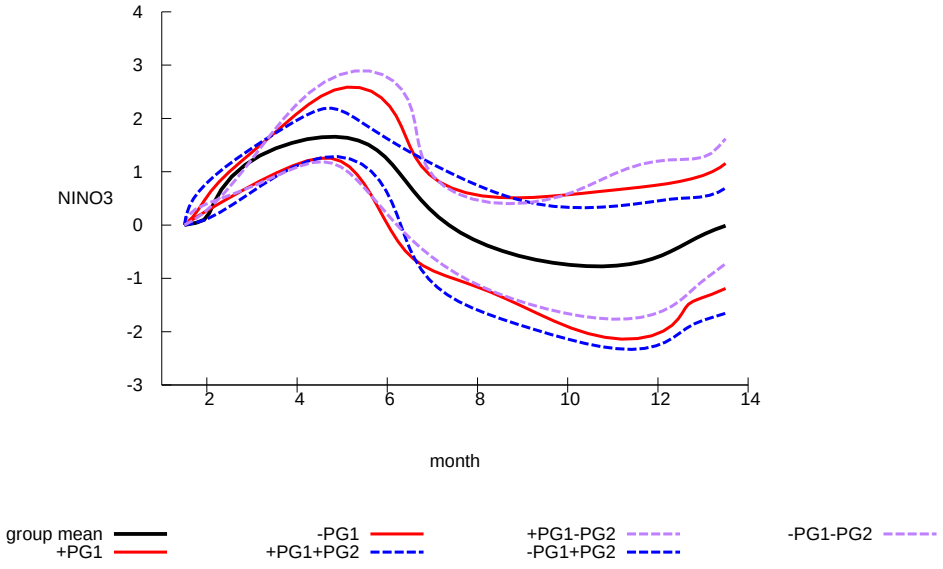

Figure 10: Principal Geodesic modes viewed as NINO3 time series

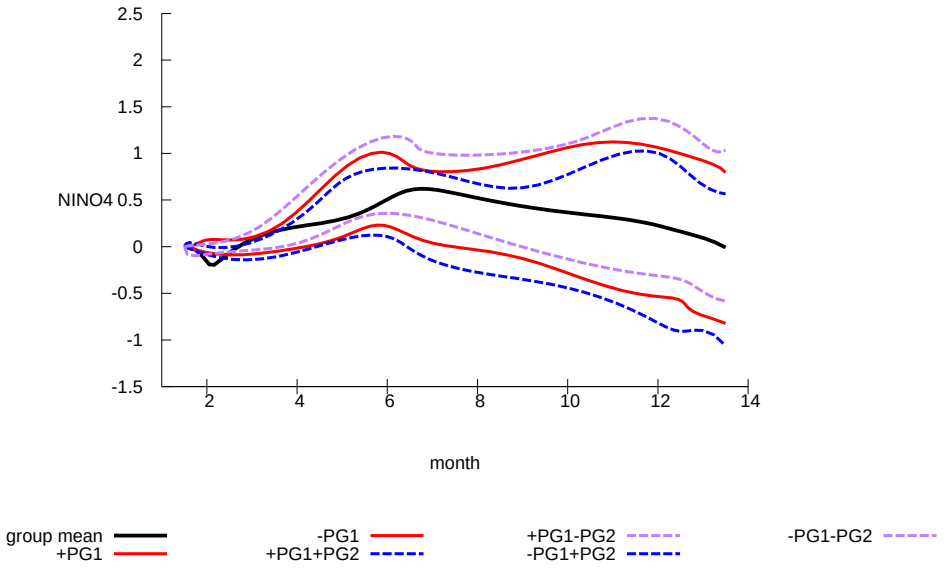

Figure 11: Principal Geodesic modes viewed as NINO4 time series

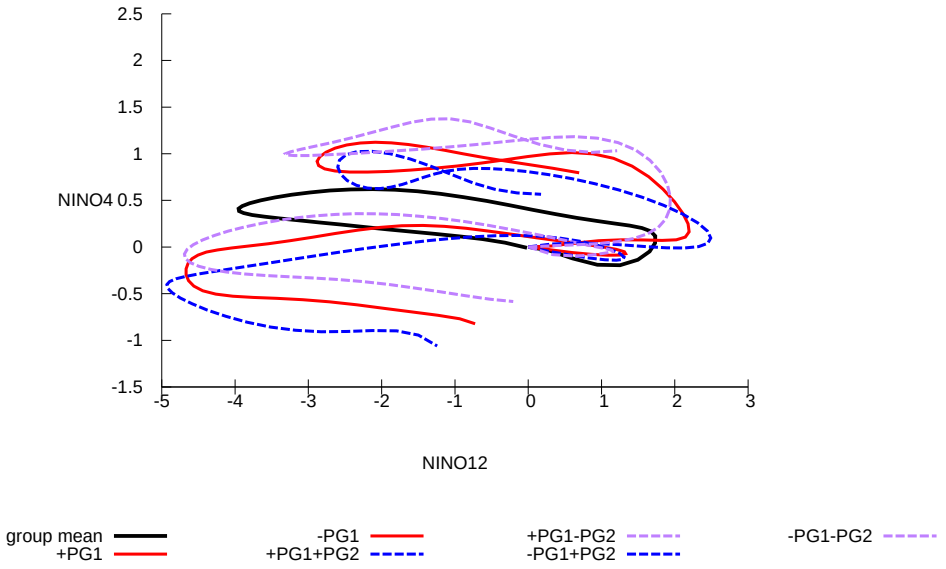

Figure 12: Principal Geodesic modes viewed as NINO12vs4 time series

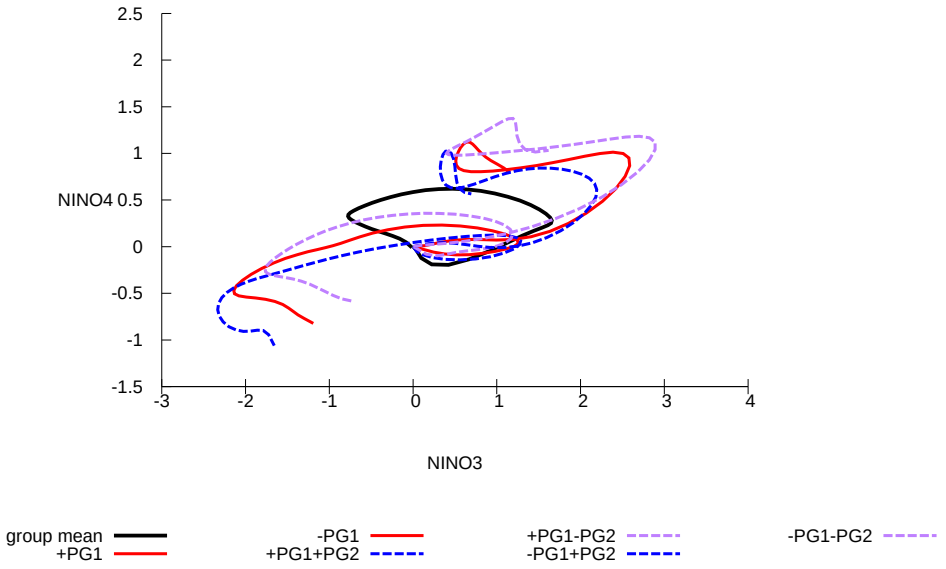

Figure 13: Principal Geodesic modes viewed as NINO3vs4 time series

4.2 Reconstruction

- **PCA** in $\mathbb{R}^{341}$ (control case #1)

$$\pi_1(x_\ell) = m + \tau_{1,\ell} u_1 + \tau_{2,\ell} u_2, \tag{27}$$
$$\tau_{i,\ell} = (u_i, x_\ell - m) \tag{28}$$

  where u_i's are eigenvectors of $\frac{1}{L}\sum_{\ell=1}^{L}(x_\ell - m) \otimes (x_\ell - m)$.

- **tPCA** (control case #2)

$$\pi_2(x_\ell) = m \exp\left(\mu_{1,\ell} w_1 + \mu_{2,\ell} w_2\right), \tag{29}$$
$$\mu_{i,\ell} = (w_i, \log\left(m^{-1} x_\ell\right)), \tag{30}$$

  where w_i's are eigenvectors of $\frac{1}{L}\sum_{\ell=1}^{L} \log\left(m^{-1}x_\ell\right) \otimes \log\left(m^{-1}x_\ell\right)$.

- **PGA** in Lie group

$$\pi(x_\ell) = m \exp\left(t_{1,\ell} v_1 + t_{2,\ell} v_2\right), \tag{31}$$

  where $t_{i,\ell}$ and v_i are the solutions of Eqs. (18) and (19).

Reconstructed time series with the first two leading modes are shown in Figs. 16, 17, 18, 19, and 20.

5 Discussion

5.1 Reconstruction errors

To compare the efficacy of the mode detection, we plot the reconstruction errors by measuring a distance between the projection onto the first two modes and the original data. Here, the error for resonstructed signature $\pi(x)$ is defined naively as a homogenous norm (c.f., Ex. 7.38 of Friz and Victoir, 2010):

$$\epsilon^2 = \|x - \pi(x)\|^2 := \sum_{k=1}^{4} \left[k! \sum_{i_1,\cdots,i_k=1}^{d} \left(x^{(i_1\cdots i_k)} - \pi(x)^{(i_1\cdots i_k)} \right)^2 \right]^{1/k}. \tag{32}$$

The points in Fig. 14 are mainly distributed in the upper left region, which shows on the whole the reconstruction by PGA is better than that by PCA or tPCA. Note that the reconstruction from PCA does not necessarily satisfies the shuffle relation.

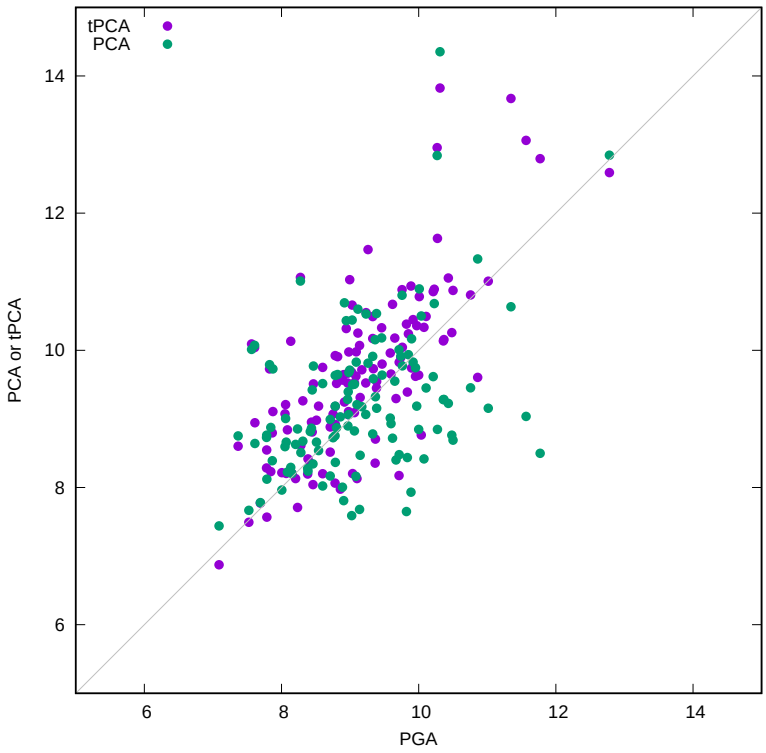

Figure 14: Comparison of the reconstruction errors for PGA vs PCA or tPCA. Each point x represents the error $\epsilon = \|x - \pi(x)\|$, refer to Eq. (32) for definition, where x is a signature of 1year-path from the climate data.

5.2 El Ninô modes

- Obviously, PG1 and PG1±PG2 are considered as El Ninõ modes (Fig. 10 and 11).
- The El Ninõ modes have characteristic undulations in May (Fig. 11) that could indicate the early signs of upcoming El Ninõ events.
- Regarding El Ninõ modes in PCA (Fig. 8) and PGA (Fig. 13), we see time goes counterclockwise and then clockwise in PG1 and PG1±PG2. Such feature is seen more clearly in PGA than in PCA.
- This should reflect the status of ocean climate that the seasonal propagation of positive temperature anomaly goes from West to East, whereas the ENSO-related one goes from East to West due to the equatorial Kelvin waves (Fig. 15), and the direction may depend on the balance of intensities between the two.

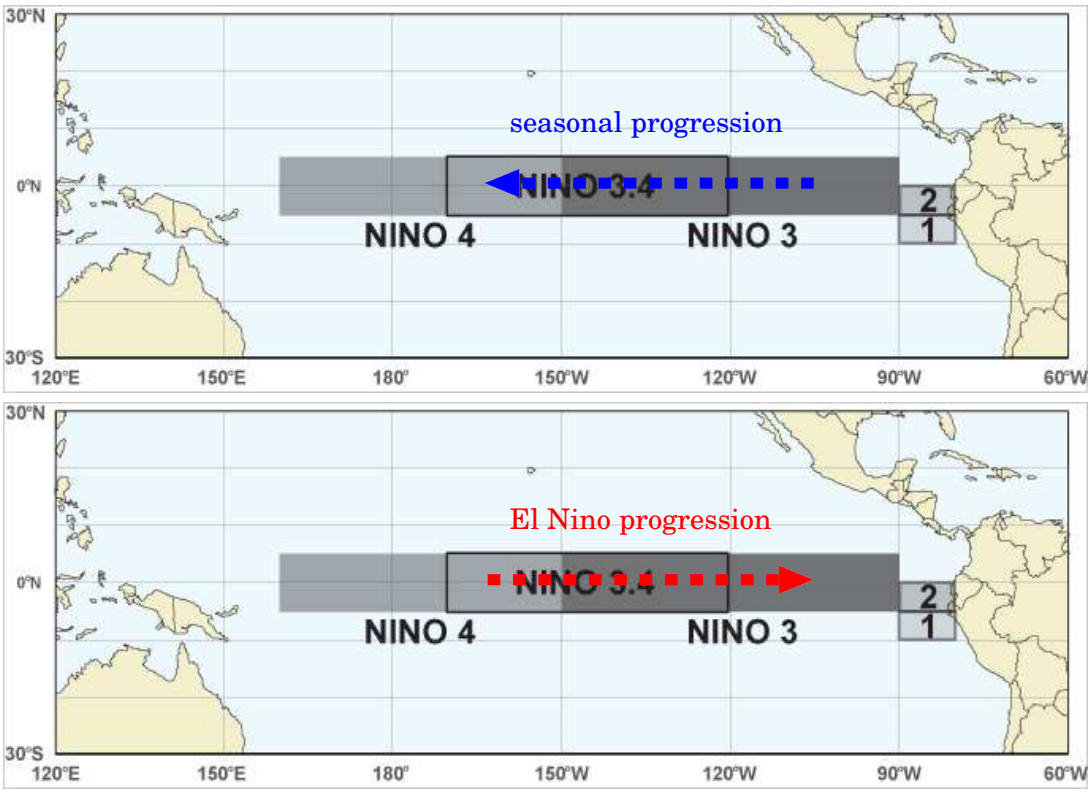

Figure 15: NINO SST regions and propagation of anomalies (original map from NOAA/PSL, 2023).

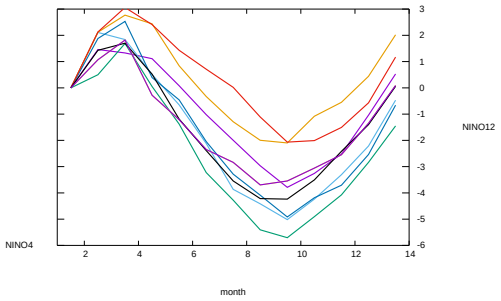

samples from real data

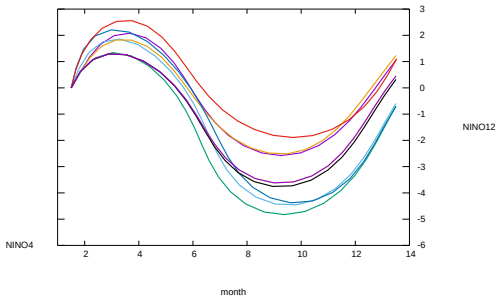

projection onto 2PCs

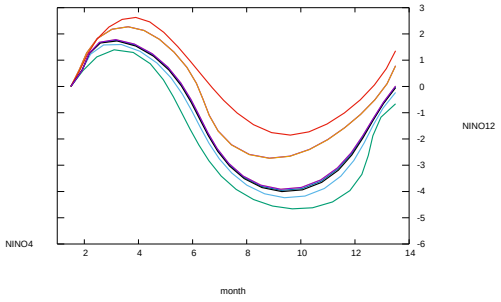

projection onto 2PGs

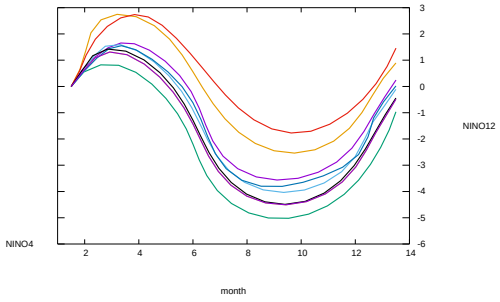

projection onto 2tPCs

Figure 16: Several samples with their projections (NINO1+2)

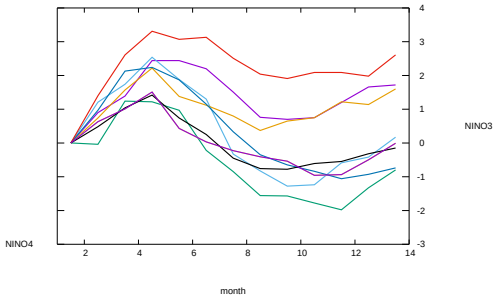

samples from real data

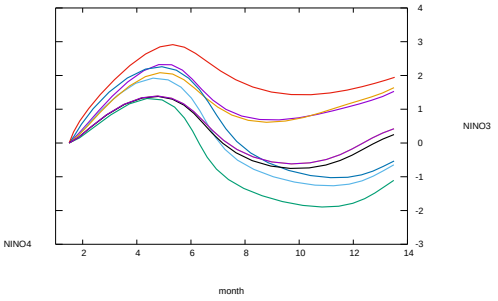

projection onto 2PCs

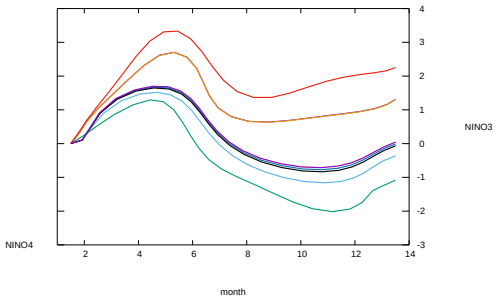

projection onto 2PGs

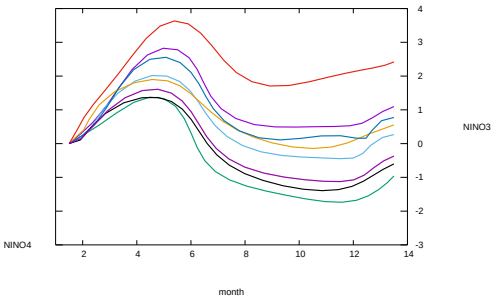

projection onto 2tPCs

Figure 17: Several samples with their projections (NINO3)

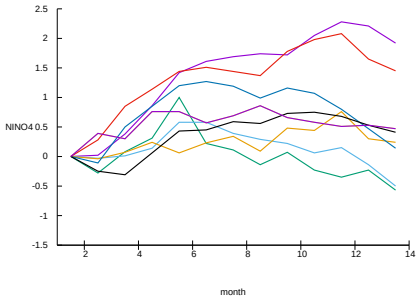

samples from real data

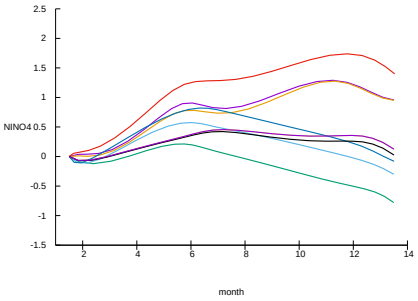

projection onto 2PCs

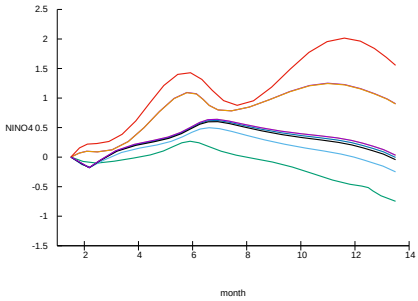

projection onto 2PGs

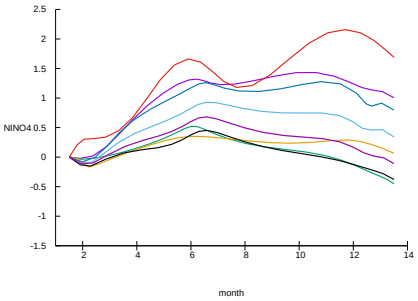

projection onto 2tPCs

Figure 18: Several samples with their projections (NINO4)

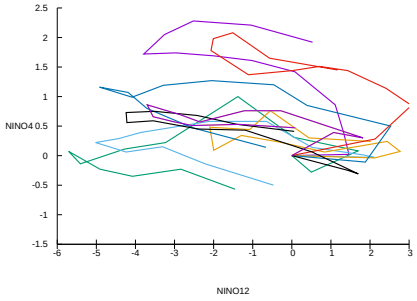

samples from real data

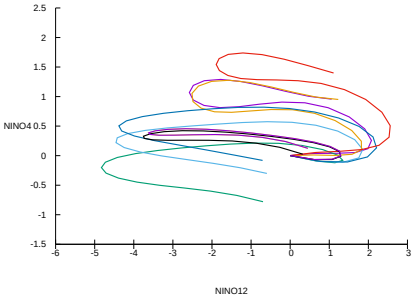

projection onto 2PCs

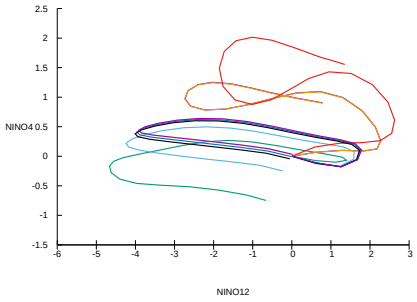

projection onto 2PGs

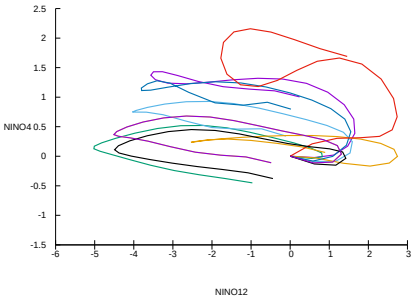

projection onto 2tPCs

Figure 19: Several samples with their projections (NINO1+2 vs 4)

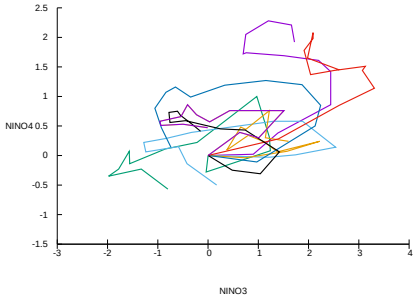

samples from real data

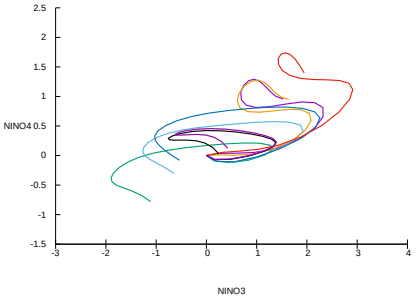

projection onto 2PCs

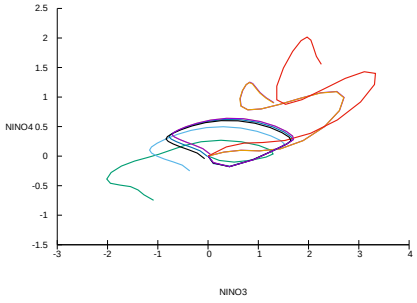

projection onto 2PGs

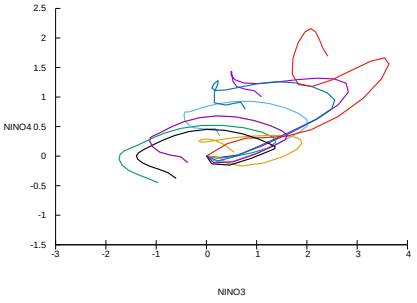

projection onto 2tPCs

Figure 20: Several samples with their projections (NINO3 vs 4)

6 Conclusion

- We applied Pennec's theory to the Principal Geodesic Analysis (PGA) for the path signatures.
- By this method, the group mean and the leading eigen modes can be identified by iterations for given time series data.
- We demonstrated the PGA with climate time series, and successfully identified the climatological mean and the first two leading variations.
- Our result offers the first example of rigorous analysis for the principal modes of sequential data.

7 Acknowledgments

This study was funded by JST-PROJECT-20218919.

References

Cogliati, A. and Mastrolia, P. (2018). Cartan, Schouten and the search for connection. *Historia Mathematica*, 45(1):39–74.

Fletcher, P. T., Lu, C., Pizer, S. M., and Joshi, S. (2004). Principal geodesic analysis for the study of nonlinear statistics of shape. *IEEE transactions on medical imaging*, 23(8):995–1005.

Friz, P. K. and Victoir, N. B. (2010). *Multidimensional stochastic processes as rough paths: theory and applications*, volume 120. Cambridge University Press.

Gámez, A. J., Zhou, C., Timmermann, A., and Kurths, J. (2004). Nonlinear dimensionality reduction in climate data. *Nonlinear Processes in Geophysics*, 11(3):393–398.

Guigui, N., Miolane, N., Pennec, X., et al. (2023). Introduction to Riemannian Geometry and Geometric Statistics: from basic theory to implementation with Geomstats. *Foundations and Trends® in Machine Learning*, 16(3):329–493.

Lyons, T. J., Caruana, M., and Lévy, T. (2007). *Differential Equations Driven by Rough Paths*, volume 1908 of *Lecture Notes in Mathematics*. Springer.

NOAA (2021). Climate Timeseries at PSL.

NOAA/PSL (visited on Mar 2023). El Ninõ Southern Oscillation (ENSO). `https://psl.noaa.gov/enso/img/oceanic-indices-map.gif`.

Pearson, K. (1901). LIII. On lines and planes of closest fit to systems of points in space. *The London, Edinburgh, and Dublin philosophical magazine and journal of science*, 2(11):559–572.

Pennec, X. and Arsigny, V. (2013). Exponential barycenters of the canonical cartan connection and invariant means on lie groups. *Matrix information geometry*, pages 123–166.

Pennec, X. and Lorenzi, M. (2020). Beyond Riemannian geometry: The affine connection setting for transformation groups. In *Riemannian Geometric Statistics in Medical Image Analysis*, pages 169–229. Elsevier.

Reizenstein, J. (2017). Calculation of iterated-integral signatures and log signatures. *arXiv preprint arXiv:1712.02757*.

Sommer, S., Lauze, F., and Nielsen, M. (2014). Optimization over geodesics for exact principal geodesic analysis. *Advances in Computational Mathematics*, 40:283–313.

Stephenson, D. and Benestad, R. E. (2000). Environmental statistics for climate researchers. *Tutorial) Version*, 14:2006.

A Why the gradient of distance squared is logarithm?

A.1 Canonical Cartan-Schouten Connection

We assume that the Lie group G is endowed with the canonical Cartan-Schouten connection (hereafter, CCS) (e.g., Cogliati and Mastrolia, 2018). Namely, the covariant derivative under CCS, $\nabla^{(0)}$, is determined by $\nabla^{(0)}_a b = \frac{1}{2}[a, b]$ for $a, b \in T_eG$.

A.2 Geodesic starting from the origin $e \in G$

Then, the geodesic starting from the origin $e \in G$ with initial velocity $v \in T_eG$ is $\gamma_v(t) = \exp(tv)$, where exp is exponential map in Lie group. This is nothing but a one parameter subgroup. Indeed, since $\nabla^{(0)}$ is a bi-invariant connection, we have the following auto-parallelism.

$$\begin{aligned}\nabla^{(0)}_{\dot\gamma_v(t)}\dot\gamma_v(t) &= \nabla^{(0)}_{dL_{\gamma_v(t)}\dot\gamma(0)} dL_{\gamma_v(t)}\dot\gamma_v(0) = dL_{\gamma_v(t)}\nabla^{(0)}_{\dot\gamma_v(0)}\dot\gamma_v(0) \\ &= dL_{\gamma_v(t)}\frac{1}{2}[\dot\gamma_v(0), \dot\gamma_v(0)] = dL_{\gamma_v(t)}\frac{1}{2}[v, v] = 0,\end{aligned} \tag{A.33}$$

where $dL_{\gamma_v(t)}$ is the derivative of left translation by $\gamma_v(t)$.

A.3 Geodesic starting from $a \in G$

Furthermore, for $a \in G$ and $v \in T_eG$, $\gamma(t) = a\exp^{(tv)}$ is a geodesic starting from a Indeed, because of $\dot\gamma(t) = dL_a\dot\gamma_v(t)$ and Eq. (A.33), we have the following auto-parallelism.

$$\nabla^{(0)}_{\dot\gamma(t)}\dot\gamma(t) = dL_a\nabla^{(0)}_{\dot\gamma_v(t)}\dot\gamma_v(t) = 0. \tag{A.34}$$

Note that we can also write the geodesic as

$$\gamma(t) = a\exp(tdL_{a^{-1}}\dot\gamma(0)) \tag{A.35}$$

by using $\dot\gamma(0) \in T_aG$ (Theorem 5.9 in Pennec and Lorenzi, 2020).

A.4 Definition of $\mathrm{Log}_a(b)$ in Geodesic manifold

Since a geodesic is described by a second-order ODE, initial point $\gamma(0)$ and terminal point $\gamma(1)$ uniquely determine a geodesic. For such geodesic, we define the initial velocity as

$$\mathrm{Log}_{\gamma(0)}(\gamma(1)) := \dot\gamma(0). \tag{A.36}$$

Inversely, the terminal point is defined as

$$\mathrm{Exp}_{\gamma(0)}(\dot\gamma(0)) := \gamma(1). \tag{A.37}$$

A.5 Log in Lie group

From Eqs. (A.35) and (A.36), we have

$$\mathrm{Log}_a(b) = dL_a\log(a^{-1}b), \tag{A.38}$$

for $a, b \in G$ and logarithm map, log, in Lie group.

A.6 Log in signature space

Suppose G is a signature space. By using the left translation by a of curve $\exp(tv)$, which has initial velocity v, the derivative of the left translation reads

$$dL_a v = \frac{d}{dt}L_a\exp(tv)|_{t=0} = \frac{d}{dt}a(1+tv)|_{t=0} = av, \tag{A.39}$$

for signature $a \in G$, log-signature $v \in T_eG$, and exponential map, exp, in tensor algebra.
From Eqs. (A.38) and (A.39), we get

$$\mathrm{Log}_a(b) = a\log(a^{-1}b), \tag{A.40}$$

for signatures a and b, and logarithm map, log, in tensor algebra.

A.7 Gradient of Squared Distance

As proven in Appendix B, we have the following property for general Riemannian manifold:

$$\nabla_a d^2(a,b) = -2\,\mathrm{Log}_a(b). \tag{A.41}$$

Combining Eq. (A.41) with Eq. (A.40), we get

$$\nabla_a d^2(a,b) = -2a\log\left(a^{-1}b\right), \tag{A.42}$$

for signatures a and b, and logarithm map, log, in tensor algebra.

B Gradient of Squared Distance

B.1 Variation of Energy

Let $\gamma : [a,b] \to M$ be a smooth curve, and $f : [a,b] \times (-\epsilon,\epsilon) \to M$ be a smooth map ($\epsilon > 0$) such that $f(t,0) = \gamma(t)$ for all $t \in [a,b]$. Energy functional is defined as $E(\gamma) = \frac{1}{2}\int_a^b |\dot\gamma(t)|^2 dt$.

Then, we have the first variation:

$$\begin{aligned}
\frac{dE(\gamma_s)}{ds} &= \frac{1}{2}\frac{d}{ds}\int_a^b \langle f_t, f_t\rangle\, dt = \int_a^b \langle \nabla_{f_s} f_t, f_t\rangle\, dt \\
&= \int_a^b \langle \nabla_{f_t} f_s, f_t\rangle\, dt \\
&= \int_a^b \frac{d}{dt}\langle f_s, f_t\rangle\, dt - \int_a^b \langle f_s, \nabla_{f_t} f_t\rangle\, dt \quad \because \text{integration by parts} \\
&= \langle f_s, f_t\rangle(b,s) - \langle f_s, f_t\rangle(a,s) - \int_a^b \langle f_s, \nabla_{f_t} f_t\rangle\, dt,
\end{aligned} \tag{B.43}$$

where ∇ is covariant derivative, and $\gamma_s := f(\cdot, s)$, and f_s and $f_t : [a,b] \times (-\epsilon,\epsilon) \to T_\bullet M$ are defined as $f_s = df\left(\frac{\partial}{\partial s}\right)$ and $f_t = df\left(\frac{\partial}{\partial t}\right)$, respectively.

In particular, if γ_s are geodesics, and the endpoint at $t = b$ is fixed, we have

$$\left.\frac{dE(\gamma_s)}{ds}\right|_{s=0} = -\langle f_s(a,0), \dot\gamma(a)\rangle\,. \tag{B.44}$$

B.2 Length vs Energy

For the length $L(\gamma) = \int_a^b |\dot\gamma(t)|dt$ of curve $\gamma : [a,b] \to M$, we have

$$L(\gamma)^2 \le 2(b-a)E(\gamma). \tag{B.45}$$

In particular, the equality is achieved when γ is a geodesic.

B.3 Distance and geodesic

If γ is a geodesic, we have $d(\gamma(a),\gamma(b)) = L(\gamma)$.

B.4 Variation of squared distance

Hence, applying Eqs. (B.44) and (B.45) to geodesics γ_s with $a = 0,\ b = 1$ and $\gamma_s(0) = m(s)$ (variable), $\gamma_s(1) = x$ (fixed), we have

$$\begin{aligned}
\left.\frac{d}{ds}d^2(m(s),x)\right|_{s=0} &= 2\left.\frac{d}{ds}E(\gamma_s)\right|_{s=0} = -2\left\langle \frac{dm}{ds}(0), \mathrm{Log}_m x\right\rangle \\
&= \left\langle \frac{dm}{ds}(0), -2\,\mathrm{Log}_m x\right\rangle.
\end{aligned} \tag{B.46}$$

B.5 Gradient of squared distance

In Eq. (B.46), the second term in the bracket is nothing but the gradient with respect to the first variable in the distance, which implies

$$\nabla_m d^2(m,x) = -2\,\mathrm{Log}_m\, x. \tag{B.47}$$

Intuitively, this means that the distance increases the most in the tangential direction of the geodesic (Fig. 21).

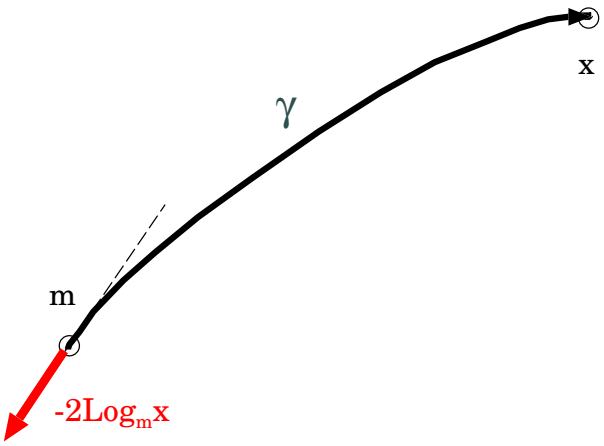

Figure 21: The distance increases the most in the tangential direction of the geodesic.

C Independence on dilation

C.1 Lagrangian

First, we rewrite Eqs. (12) and (13) with Lagrange multipliers $\zeta_\ell \in \mathcal{T}_n^*(\mathbb{R}^d),\ \ell = 1, \cdots, L$ as Lagrangian:

$$\mathcal{L}(\{t_\ell\}, v, \{p_\ell\}, \{\zeta_\ell\}) = \sum_{\ell=1}^{L} d^2(p_\ell, x_\ell) + \sum_{\ell=1}^{L} \left(\zeta_\ell, p_\ell - m\mathrm{e}^{t_\ell v}\right), \tag{C.48}$$

where $(,)$ is the dual product.

Then, the stationary problem reads

$$\forall \ell) \quad \nabla_{p_\ell}\mathcal{L} = -2p_\ell \log\left(p_\ell^{-1}x_\ell\right) + \nabla_{p_\ell}\left(\zeta_\ell, p_\ell\right) = 0, \tag{C.49}$$

$$\forall \ell, I) \quad \frac{\partial \mathcal{L}}{\partial \zeta_\ell^{(I)}} = \left[p_\ell - m\mathrm{e}^{t_\ell v}\right]^{(I)} = 0, \tag{C.50}$$

$$\forall \ell) \quad \frac{\partial \mathcal{L}}{\partial t_\ell} = -\left(\zeta_\ell, \frac{\partial\left[m\mathrm{e}^{t_\ell v}\right]}{\partial t_\ell}\right) = 0, \tag{C.51}$$

$$\forall I) \quad \frac{\partial \mathcal{L}}{\partial v^{(I)}} = -\sum_{\ell=1}^{L}\left(\zeta_\ell, \frac{\partial\left[m\mathrm{e}^{t_\ell v}\right]}{\partial v^{(I)}}\right) = 0, \tag{C.52}$$

where (I) is a multi-index in $\mathcal{T}_n(\mathbb{R}^d)$.

C.2 Dilated solution

Applying the dilation δ_λ by $\lambda > 0$ to Eqs. (C.49) and (C.50), and considering compensation $\delta_{\lambda^{-1}}$ in the dual products in Eqs. (C.49), (C.51), and (C.52), we have

$$-2(\delta_\lambda p_\ell)\log\left((\delta_\lambda p_\ell)^{-1}\delta_\lambda x_\ell\right) + \nabla_{\delta_\lambda p_\ell}\left(\delta_{\lambda^{-1}}\zeta_\ell, \delta_\lambda p_\ell\right) = 0, \tag{C.53}$$

$$\delta_\lambda p_\ell - (\delta_\lambda m)\mathrm{e}^{t_\ell \delta_\lambda v} = 0, \tag{C.54}$$

$$-\left(\delta_{\lambda^{-1}}\zeta_\ell, \frac{\partial\left[(\delta_\lambda m)\mathrm{e}^{t_\ell\delta_\lambda v}\right]}{\partial t_\ell}\right) = 0, \tag{C.55}$$

$$-\sum_{\ell=1}^{L}\left(\delta_{\lambda^{-1}}\zeta_\ell, \frac{\partial\left[(\delta_\lambda m)\mathrm{e}^{t_\ell\delta_\lambda v}\right]}{\partial v^{(I)}}\right) = 0, \tag{C.56}$$

where we used the fact that the dilation is a homomorphism in the tensor algebra.

Equations (C.53)–(C.56) imply that if data were $\{\delta_\lambda x_\ell\}$, we should have solution $(\{t_\ell\}, \delta_\lambda v)$, which means that the solution to problems (12) and (13) is consistent under the dilation to the signature.

D Gradient in Embedded space

Because the signature space G is embedded in $\mathbb{R}^N$ with $N = (d^{n+1}-1)/(d-1)$, the gradient on T_eG is represented as the derivative in $\mathbb{R}^N$ projected onto T_eG. Noting that $p = p(t,v) = m\mathrm{e}^{tv}$ is ristricted on G, we have

$$\begin{aligned}\nabla_v d^2(p(t,v),x) &= \operatorname*{proj}_{T_eG}\left[\frac{\partial d^2(p,x)}{\partial v}\right]^\top = \operatorname*{proj}_{T_eG}\left[\frac{\partial d^2(p,x)}{\partial p}\frac{\partial p}{\partial v}\right]^\top \\ &= \operatorname*{proj}_{T_eG}\left[\left(\frac{\partial p}{\partial v}\right)^\top \operatorname*{proj}_{T_pG}\left(\frac{\partial d^2(p,x)}{\partial p}\right)^\top\right] = \operatorname*{proj}_{T_eG}\left[\left(\frac{\partial p}{\partial v}\right)^\top \nabla_p d^2(p,x)\right],\end{aligned} \tag{D.57}$$

where $v \in T_eG$, and $\mathrm{proj}_{T_eG} : \mathbb{R}^N \to T_eG$ and $\mathrm{proj}_{T_pG} : \mathbb{R}^N \to T_pG$ are projection operators. On the other hand, the derivative with respect to t is just

$$\nabla_t d^2(p(t,v),x) = \left(\frac{\partial p}{\partial t}\right)^\top \nabla_p d^2(p,x). \tag{D.58}$$

In these equations, we can compute $\left(\frac{\partial p}{\partial v}\right)^\top$ and $\left(\frac{\partial p}{\partial t}\right)^\top$ by automatic differentiation.